Contributions of natural climate variability on the trends of seasonal precipitation extremes over China

Fuqiang Cao [1, 2], Tao Gao [3, 4*], Li Dan[2], Fengxia Zhao[1], Xiang Gong[5], Xinyu Zhang[6], Xiaoyu Long[7] and Junjie Zhan[8]

[1] School of geosciences, Shanxi Normal University, Linfen 041000, China

[2] CAS Key Laboratory of Regional Climate-Environment Research for Temperate East Asia, Institute of Atmospheric Physics, Chinese Academy of Sciences, Beijing, China

[3] College of Urban Construction, Heze University, Heze 274000, China

[4] State Key Laboratory of Numerical Modeling for Atmospheric Sciences and Geophysical Fluid Dynamics, Institute of Atmospheric Physics, Chinese Academy of Sciences, Beijing 100029, China

[5] School of Mathematics and Physics, Qingdao University of Science and Technology, Qingdao 266061, China

[6] College of Graduate Studies, Sul Ross State University, Alpine Texas, USA 79832

[7] Joint Institute for Marine and Atmospheric Research, School of Ocean and Earth Science and Technology, University of Hawai‘i at Mānoa, Honolulu, Hawaii, USA

[8] Shunyi Meteorological Service, Beijing, 101300, China

∗ To whom all correspondence should be addressed to: Dr./Prof. Tao Gao (tgao.oc@gmail.com)

This article has been accepted for publication and undergone full peer review but has not been through the copyediting, typesetting, pagination and proofreading process which may lead to differences between this version and the Version of Record. Please cite this article as doi: 10.1002/joc.7126

Abstract

The increased trends of extreme precipitation events over China have been partially attributed to global warming, while it is unclear how the natural climate variability affect these variations in extreme rainfall trends. Here we examine the contributions of large-scale modes climate variability from the Pacific Ocean, which are represented by El Niño-Southern Oscillation (ENSO) and Pacific Decadal Oscillation (PDO), on the trends of seasonal extreme events across China. Results show that the effects of climate variability modes on precipitation extremes exhibit evidently spatiotemporal characteristics at the seasonal scale. A significant positive trend is found over southeastern and northwestern China in four seasons, and substantial increases in two types of extreme events are also seen over northwestern China in spring and winter. Most of the seasonal trends of extreme precipitation events can be explained by the trends of the principal components. El Niño (La Niña) and PDO–like Sea Surface Temperature (SST) anomalies over the Pacific have a close linkage with the variations in precipitation extremes. By modulating the large-scale atmospheric circulations, these Pacific SST anomalies associated with climatic oscillations, such as ENSO and PDO, provide the conducive conditions responsible for the occurrences of seasonal precipitation extremes across China. The seasonal trends of extreme events can be largely explained by the variability of the ENSO and PDO episodes, with a relatively larger modulation of PDO as compared to ENSO. These researches have important implications for improving seasonal flood disaster predictability and climate model performances.

Key words: climate variability modes; extreme precipitation events; seasonal trends; El Niño-Southern Oscillation; Pacific Decadal Oscillation;

1 Introduction

Extreme precipitation events are defined as the rainfall events occur low frequently at a given scale. However, once the extreme events happen, they often trigger devastating impacts on eco-environment system and human activities, and even the more losses caused by secondary disasters such as mudslides, floods, landslides, and city waterlogging (e.g., Easterling et al., 2000; Alexander et al., 2006; You et al., 2011; Donat et al., 2016; Miao et al., 2018). For example, the torrential rainfall over Beijing on July 21, 2012 caused 79 casualties, with the estimated economic losses more than 10 billion RMB (Sun and Zhang, 2017). The persistent intense rainfall from July 8 to 11 in 2013 in the Sichuan Basin reached an accumulated rainfall of 721.4 mm, leading to serious floods (Wang et al., 2013). It is therefore of tremendous importance to better understand the past changes in precipitation extremes and the underlying mechanisms. This is critical for the reliable future projections of extreme precipitation variations and response of the hydrological cycle to global climate warming.

Previous studies have documented the changes in trends of extreme precipitation events in the whole country and selected regions across China. Generally, the intensity and amount as well as frequency of precipitation extremes exhibited an increasing trend in China, meanwhile, the variations in extreme events are correlated to the total rainfall changes (Zhai et al., 2005; Gao and Xie, 2016; Gao and Wang, 2017; Sun and Zhang, 2017; Xiao et al., 2017). Spatially, extreme precipitation trends show apparently regional characteristics in different areas of China. Increased amount of intense precipitation events are discovered over Northwest China and the mid-lower reaches of

the Yangtze River basin (YRB), whereas, declined trends of extremes are distributed over North China and Sichuan Basin (Zhai et al., 2005; Chen and Zhai, 2015; Gao et al., 2016; Cao et al., 2019). These regional differences are also coincident with the changes in the frequency of extreme precipitation events (Gao and Xie, 2016; Guan et al., 2017). The extreme precipitation amount and its proportion of the total rainfall display an increasing trend over the northern portion of eastern China, and the declining trends are mainly located in the south of eastern China, particularly over the mid-lower reaches of the YRB and North China (Sun, 2012; Wang et al., 2016; Gao et al., 2017; Wang et al., 2019). Remarkable increases in summer total rainfall, the frequency and intensity of extreme precipitation events are seen in the mid-lower reaches of the YRB. In Northwest China, 70% of the meteorological stations exhibit an increase in the intensity of extreme events (Jiang et al., 2013; Wang et al., 2019). Fifth Assessment Report of the Intergovernmental Panel on Climate Change (IPCC AR5) argued that those regional trends of rainfall anomalies across China are jointly affected by human forcing and atmospheric circulations.

The recent studies focusing on the contribution of regional precipitation extremes have been centered on the forcing factors of human activities. Particularly, anthropogenic aerosols impact precipitation features through the absorption and scattering of incoming solar radiation, furthermore, aerosols also cool the surface and offset the greenhouse gases-induced warming and thereby its influences on rainfall (Chen et al., 2011; Rosenfeld et al., 2014; Liu et al., 2015; Lin et al., 2016; Fan et al., 2016; Ma et al., 2017). Min et al. (2011) and Zhang et al. (2013) argued that human-

induced greenhouse gas increases had a detectable influence on the observed intense rainfall events during second half of twentieth century, and also on the intensification of observed hydrologic cycle after the 1980s (Min et al., 2011; Westra et al., 2013; Zhang et al., 2013; Lehmann et al., 2015). In addition to the anthropologic forcing factors, nature variability of the climate system, for example, ENSO and PDO, has also been proved to contribute the variations in occurrences of extreme precipitation events (Si and Ding, 2016; Gao et al., 2017; Yan et al., 2020; Gao et al., 2020). The well-documented correlations between seasonal intense precipitation over China and the positive (negative) phase of ENSO have been investigated in prior studies. Generally, the heavy rainfall in southern (northern) China increases (decreases) in winter and autumn in El Niño years, and summer intense precipitation over the northern regions of Yellow River basin decreases during El Niño episodes (Gong and Wang, 1999; Wang et al., 2000; Xiao et al., 2015).

However, existing studies mainly focused on the effects of climate variability modes on the frequency (e.g., Wang and Yan, 2011; Li et al., 2012), interdecadal shifts (e.g., Wang et al., 2013; Xu et al., 2015; Gao et al., 2016) and spatial patterns (e.g., Zhai et al., 2015; Sun and Zhang, 2017) of extreme precipitation events across China, few of them have linked the trends of precipitation extremes to natural climate variability. In this study, we further examine the trends of seasonal precipitation events over China, with a particular focus on the understanding of what physical mechanisms responsible for these changing trends derived from interannual and interdecadal climate system variability. To comprehensively analyze the impacts of large-scale modes of climate

variability on different magnitudes of extreme precipitation regimes, percentile and absolute definitions of extreme precipitation events are utilized to characterize the intense and persistent features of precipitation extremes. The remainder text is organized as follows. The dataset and methods employed in this study are introduced in section 2. The results are presented in section 3, followed by conclusion and discussion in section 4.

2 Data and methods

Extreme precipitation events across China are defined by the gridded observational rainfall dataset of CN05.1 from 1961 to 2016 at the daily scale (Wu and Gao, 2013). CN05.1 is obtained by construction based on 2416 station observations with a high spatial resolution of 0.25°×0.25°. In particular, this dataset is interpolated by utilizing the 'anomaly approach' (New et al., 2002). The thin-plate smoothing splines are first applied to calculate mean climatology during 1971-2000, then the gridded daily anomalies obtained through the angular weighting method are added to it. CN05.1 includes four variables, daily mean, minimum and maximum temperature, as well as cumulative precipitation. This gridded dataset with high resolution is suitable to examine the observed climatic features and assess the global and regional model performances (Sun and Wang, 2015; Cao and Gao, 2019; Cao et al., 2019). Similar to other gridded rainfall products, the accuracy of the CN05.1 at a selected time and location is subject to the availability and quality of observed precipitation data, which vary temporally and spatially based on the heterogeneity of instrument platforms, record lengths and spatial coverage. While CN05.1 with a higher spatial resolution is

more suitable for our analysis purpose as compared to other available gridded rainfall datasets.

To synthetically examine different magnitudes of extreme precipitation events associated with climate variability modes, percentile and duration threshold approaches are applied to define extreme events in spring (March to May, MAM), summer (June to August, JJA), autumn (September to November, SON), and winter (December to February, DJF), respectively. The seasonal 90th percentile of precipitation distribution is utilized as threshold for defining extreme precipitation events at each gridded site in the same season. That is, an extreme event is considered when the daily cumulative rainfall amount exceeds the 90th percentile (R90p) of each season for the entire period. The seasonal maximum consecutive 5-day precipitation (RX5day) is employed to feature the duration of extreme events. In addition, seasonal total rainfall is also used to further analyze the different effects of large-scale modes on extreme precipitation events and total rainfall over China. We principally investigate the seasonal trends of these two types of extreme precipitation regimes and their possible causes associated with large-scale atmospheric circulations.

The reanalysis datasets of geopotential height at 500 hPa, wind field at 850 hPa, and 2-m temperature available at 1.25° × 1.25° resolution from 1961 to 2014, are obtained from the 55-year Japanese Reanalysis Project (JRA-55; http://jra.kishou.go.jp/JRA-55/index_en.html; Harada et al., 2016). As the JRA-55 is better for representing the variations in drought indices over China in comparison with other available reanalysis datasets (Chen et al., 2019). Sea Surface Temperature (SST) dataset is obtained from

the Hadley Centre, Met Office (Rayner et al., 2003). The monthly El Niño-Southern Oscillation (ENSO) index (Hoerling et al., 2001) is defined by 3 month running mean of SST anomalies in the Niño 3.4 region and presented by Oceanic Niño Index (ONI), it is available from the website (https://origin.cpc.ncep.noaa.gov/products/analysis_monitoring/ensostuff/ONI_v5.php). And the monthly Pacific Decadal Oscillation (PDO) index (Mantua et al., 1997) is obtained from the website (http://atmos.washington.edu/~mantua/abst.PDO.html). The empirical orthogonal function (EOF) technique is used to explore the influences of dominant patterns of the natural climate variability on seasonal precipitation extremes. Regression analysis is also applied to reveal the relationship between the trends of extreme precipitation events and anomalous ocean-atmospheric variables.

3 Results

During the last 56-yr, extreme precipitation events defined by 90th percentile threshold (R90p) generally show an increasing trend in four seasons over southeastern and northwestern China, with the distinct discrepancies for the trends of extreme events at the seasonal scale. (Fig. 1). In spring and winter, the statistically significant positive trends are mainly found in southeastern, northeastern and northwestern China (Fig. 1a, g), with the exception of central and southwestern areas exhibiting a declining trend of precipitation extremes in spring (Fig. 1a). Correspondingly, the country-averaged extreme events at the gridded sites, where the positive trends are statistically significant at the 95% confidence level, display an increasing trend for both seasons, even though the interannual and interdecadal variability is apparent from 1961 to 2016. Note that

the variations in averaged events at the country scale exhibit large significant trends of 4.7mm/yr and 4.2mm/yr in summer and autumn, respectively (Fig. 1d, f), however, spatial distribution of the trends of extreme events is relatively more inhomogeneous in comparison with other two seasons. Declining trends are seen over southwestern, northern and northeastern China, while the strengthened increases in precipitation extremes are located over central-east China (Fig. 1b). The significant positive and negative trends of extreme events over different subregions across China lead to an insignificant country-averaged trend of summertime precipitation extremes (Fig. 1c, d). In autumn, both the positive and negative trends of extreme precipitation events are lesser significant compared to summertime changes (Fig. 1c, e), resulting in an insignificant trend of the average precipitation events in autumn for the whole country.

The variations in persistent extreme precipitation events (RX5day) share the similar features with threshold extreme events (Fig. 1-2). Statistically significant increasing trends of RX5day are principally distributed in spring and winter (Fig. 2a, g). Particularly, more evident upward trends occur in winter, this facilitates a statistically significant positive trend of the country-averaged RX5day (Fig. 2h), suggesting that wintertime persistent precipitation extremes become more enhanced across China during 1961-2016. In summer and autumn, the increasing trends of RX5day are primarily situated over western and southeastern China, while the declining trends are not significant in comparison with R90p. It is worth noting that the persistent intense events, such as RX5day, are likely to cause disastrous consequences (Chen and Zhai, 2015; Gao and Xie, 2016), these suggest that the flooding risks may, therefore, be

strengthened over China, especially in winter. Spatial distribution of the trends of seasonal total rainfall (Fig. S1) is roughly consistent with that for R90p (Fig. 1), while the time series of country-averaged precipitation extremes shows an evident trend in winter, this is coincident with RX5day. Moreover, the remarkably positive shifts occur around the 1990s in several seasons for both the total and extreme precipitation variations (Fig. 1-2 and Fig. S1), these shifts are further reconfirmed by Mann-Whitney-Pettitt test (Fig S2) (Fu et al., 2015) and have also been reported in previous studies (Ding et al., 2009; Huang et al., 2013; Gao et al., 2016; Xu et al., 2015). Meanwhile, these positive shifts might dominate the long-term country-averaged trends during entire period. In addition, previous studies demonstrated that the northwestern regions tend to be warm and wet during the last decades (Peng and Zhou, 2017; Wang et al., 2019), it is in agreement with the results in the present study.

The EOF analysis is employed separately to seasonal total and extreme precipitation events for identifying the dominant space-time patterns of their variability. The spatial patterns and principal components (PCs) of the first modes, expressed by EOF1 and PC1, respectively, for each season are shown in Fig 3-4. The total variances of R90p are 24.07%, 13.03%, 15.39%, and 53.34% in spring, summer, autumn, and winter, respectively. Figure 3 depicts that the spatial patterns of EOF1 are similar to those of extreme precipitation trends (Fig. 1). In spring, the positive anomalies are predominantly found over southern China, and the regions of negative anomalies are mainly located in central-east China, this indicates more and less occurrences of precipitation extremes in southern and central-east China, respectively (Fig. 3a). The

corresponding PC1 time series exhibits a slight upward trend with significantly large interannual and interdecadal variability (Fig. 3b). The spatial uniformity of EOF1 in summer, autumn, and winter is more evident than that for spring, distinctly positive anomalies are discovered over southern and central China in summer and autumn, respectively (Fig. 3c, e). There exists a remarkable shift around the 1990s for summertime PC time series, while the similar shifts occur around the 1980s in other three seasons (Fig. 3b, d, f, g). Considering persistent precipitation extremes, spatial pattern of positive anomalies of EOF1 generally matches with the significant increasing trends of RX5day in four seasons (Fig. 2, 4), with pronounced anomalies distributed over central-east and southeastern China. However, the total variances explained by EOF1 are relatively smaller in comparison with that for R90p, the largest explained variance occurred in winter is 32.02%, which is much less than 53.34% for wintertime RX5day. The remarkable shifts appear around the 1990s for PCs in summer and autumn, even though the interannual and interdecadal variability is relatively evident in four seasons. The spatial patterns of the EOF1 for seasonal total rainfall (Fig. S3) are approximately coincident with that for extreme precipitation events (Fig. 3, 4), with more significant positive anomalies for total rainfall and R90p compared to RX5day. Moreover, the total rainfall and R90p also display roughly similar seasonal PC time series. These suggest that the total rainfall amount at the seasonal scale over China may be dominated by longer persistent precipitation extremes in comparison with RX5day.

To reveal the explanations, which are responsible for the trends of precipitation extremes, derived from PCs. We adopt residual trends (Yu et al., 2016; Yu et al., 2018)

that can measure the explained amount of extreme precipitation trends by utilizing ratios of the residual trends to total trends. The relatively larger ratios suggest that the trends of seasonal extreme precipitation events can be lesser explained by trends of the PCs. The residual trends are defined by subtracting the seasonal PC trends from total trends. Figures. 5 and 6 depict the changes in residual trends and ratios for R90p and RX5day, respectively. The magnitudes of residual trends are relatively smaller (approximately less than 0.5mm/yr), even though there exist pronounced changes across China, particularly for RX5day, with most of regions smaller than 0.5mm/yr in four seasons. The spatial distribution of the ratios of residual trends to total trends also exhibits considerably regional characteristics. Similar to the residual trends, the ratios are also relatively small in most of seasons for both R90p and RX5day, implying that the trends of seasonal precipitation extremes can be largely explained by the PC1 trends, especially for the gridded sites with statistically significantly increasing trends of extreme events. These phenomena are roughly paralleled with residual trends and ratios of seasonal total rainfall (Fig. S4).

At the interannual and interdecadal timescales, ENSO and PDO are the major large-scale modes of climate variability over the Pacific Ocean. The seasonal ENSO index shows inconspicuous trends, but has significant interannual variability. While the PDO index exhibits increasing trends in four seasons, with remarkable shifts around 1990s (Fig. 7), this is generally coincident with the shifts of extreme and total rainfall events analyzed above. Prior studies have documented the close linkages between extreme precipitation events over China and variations in SST oscillation anomalies

characterized by the ENSO and PDO (e.g., Ouyang et al., 2014; Xiao et al., 2015; Si and Ding, 2016; Gao et al., 2017). We further examine the correlations between seasonal precipitation extremes and ENSO as well as PDO by utilizing multivariable regression (Table 1). The positive and negative regression coefficients for ONI (PDO) index indicate the corresponding relationships between the ONI (PDO) index and the PC1s. Table 1 shows that PDO yields a positive contribution to extremely large precipitation events in four seasons, while the negative contribution of PDO is found for the persistent precipitation extremes, except for spring. On the contrary, ENSO exerts a positive contribution on RX5day, and a negative effect on R90p, excluding the spring. ENSO and PDO have a negative and positive contribution, respectively, on seasonal total rainfall in summer, autumn, and winter, and negative contributions are found in spring for both climate variability modes (Table s1). Furthermore, the magnitudes of regression coefficients for PDO index are relatively larger than that for ONI index, suggesting that PDO index exerts a relatively larger contribution to the trends of the PC1s than that of the ENSO index. This also confirms that the extreme events are clearly modulated by natural climate variability.

To further examine the extreme precipitation trends explained by the PCs associated with large-scale atmospheric circulation anomalies, the SSTs, 500 hPa geopotential height, wind vector at 850 hPa and 2-m temperature are regressed to the seasonal PCs. The regression maps of the 500 hPa geopotential height show that the tropical Pacific Ocean are dominated by pronounced negative anomalies in spring, in particular over South China Sea (SCS). Meanwhile, the evident positive anomalies are located over

northern China (Fig. 8-9), combined with the significant positive SST anomalies over the SCS and an anomalous lower-level anticyclone centered over the western North Pacific (WNP) (Fig. 10), these indicate that the anomalous southwesterlies are found along the northwest flank of the anomalous anticyclonic system, which transport sufficient moisture fluxes from the tropical Pacific Ocean to the southern China, forming the conducive conditions of the occurrences of extreme precipitation events, consistent with the strengthened rainfall events there. In addition, distinct El Niño–like SST anomalies appear over the eastern tropical Pacific, and the warm phase of PDO–like SST anomalies occur over the North Pacific (Fig. 8-9). This further confirms the correlations between springtime precipitation extremes and ENSO as well as PDO as the aforementioned analyses and Table 1. In summer, southern China and SCS are controlled by negative geopotential height anomalies, and the pronounced horseshoe-like positive SST anomalies are found over the SCS and Indian Ocean. Over the eastern tropical Pacific, the spring El Niño–like SST anomalies persist to the summer.

In ensuing spring and summer during the positive phase of ENSO episodes, the SST anomalies over the eastern tropical Pacific decay rapidly, while the anticyclone over the western tropical Pacific can be maintained derived from local air–sea interaction. More notably, the northeastern wind anomalies on the east flank of the anticyclonic system enhance the climatological trade winds, strengthening the latent heat fluxes from the ocean to atmosphere and cooling their underlying SSTs. Negative SST anomalies excite the anomalous westward propagation and weaken the Rossby waves, which, in return, reinforces the anticyclonic system (Li et al., 2017; Wang and Zhang, 2002). On the west

flank of the negative SST anomalies, southerlies prevail over the western side of anticyclonic system, this transports warm air from the low-latitude oceans and contributes to the positive SST anomalies around the SCS and surrounding regions, leading to intense rainfall events over central-east China and southeastern China (Fig. 10).

At the interdecadal scale, phase transition of the PDO can affect precipitation regimes over eastern China by modulating East Asian westerly jet stream (EAWJS), which has been suggested as the bridge to correlate the Pacific SST anomalies and East Asian rainfall anomalies (Lau et al., 2004). The negative phase of PDO episodes can result in evident easterly anomalies over East Asia. Consequently, the EAWJS weakens and shifts poleward, this is coincident with the shifts of EAWJS after the late 1990s based on observational analyses (Fig. 7). Furthermore, weakened and poleward shifts of the EAWJS can lead to the anomalous ascending motions over eastern China by altering the secondary jet-related meridional-vertical circulations. As a result, in intense precipitation events increased after the late 1990s. In addition, the positive phase of Atlantic Meridional Oscillation may only induce insignificant variations over East Asia and partially offset the negative PDO effects (Zhu et al., 2015).

The above documented analyses are also depicted in Figs. 8-10 and Fig. S5-6, this demonstrates that the contributions of natural climate variability on the seasonal trends of precipitation extremes across China are apparent. The geopotential height anomalies at 500 hPa in autumn and winter also facilitate the water vapor transports into China, consistent with the regression maps of wind fields. The El Niño–like SST anomalies in

summer are followed by La Niña–like SST anomalies in autumn, and the slightly weakened El Niño–like SST anomalies re-develop in winter. Meanwhile, the slightly weak PDO–like SST anomalies also accompany over the Pacific, since previous studies have reported that the ENSO-related teleconnections with precipitation extremes over China can be modulated by PDO modes, and the superposition of the influences of ENSO and PDO alter the variations in extreme events (Chan and Zhou, 2005; Cai et al., 2011; Si and Ding, 2016). Given that temperature anomalies play an important role on the changes in extreme precipitation regimes at the regional and local scales (Utsumi et al., 2011). Figure 11 depicts that 2-m temperature has a close linkage with R90p, consistent with the spatial pattern of seasonal total rainfall (Fig. S7). The negative correlation between 2-m temperature and precipitation extremes is located over central-east China in summer, indicating that less extreme precipitation events occur with the increased surface temperature. The positive correlations are seen over most regions of China in winter, suggesting that largely extreme rainfall events (R90p) are proportional to 2-m temperature. However, persistent precipitation extremes (RX5day) have a smaller correlation with 2-m temperature in comparison with seasonal R90p and total rainfall.

4 Conclusion and discussion

Many existing studies contribute the changes in extreme precipitation events over China, in large part, to the strengthened emission of the greenhouse gas concentrations. While the analysis in how the large-scale modes of climate variability affect the trends of precipitation extremes is still limited. Building on the previous researches, we

investigate the seasonal trends of extreme events during the last decades across China based on the high-resolution gridded rainfall dataset, and also examine the contributions of natural climate variability, such as ENSO and PDO, on the variations in trends of precipitation extremes.

Both the extreme precipitation events and annual total rainfall amount generally exhibit an increasing trend over southeastern and northwestern China in four seasons. Particularly, the statistically significant positive trends are found in northeastern China in spring and winter for R90p, but only in winter for RX5day. The declining trends of precipitation extremes are principally seen over northern and southwestern China in summer and winter. The trends of R90p, RX5day and total rainfall share a similar spatial distribution, with the relatively smaller magnitude of RX5day trends. In summer, R90p displays the largest increasing trend of country-averaged events, with the growth rate of 4.7mm/yr, this is followed by autumn trend of 4.2m/yr. Whereas, the largest trend of 2.4mm/yr appears in autumn for RX5day. It needs to be mentioned that the most statistically significant positive trend of seasonal total rainfall with the rate of 5.6mm/yr occurs in autumn, consistent with larger increases in extreme precipitation events. These suggest that the increases in seasonal total rainfall amount, to a certain extent, are modulated by variations in precipitation extremes, rather than the moderate and light rainfall events.

The spatial pattern of the first EOF modes for precipitation extremes resembles the spatial distribution of their trends, with the seasonal PC1 exhibiting significant interannual and interdecadal variability during 1961-2016. The analyses of residual

trends suggest that the extreme precipitation trends can be largely explained by the trends of the PCs at the seasonal scale over most of China.

These changes in trends and time series of PCs are found to be correlated with the SST oscillations featured by ENSO and PDO over the Pacific Ocean. In spring and summer, the evident El Niño–like (PDO–like) SST anomalies are discovered over the eastern tropical (North) Pacific, combined with the significant positive anomalies of 500 hPa geopotential height over the tropical Pacific Ocean and SCS, these are associated with an anomalous lower-level anticyclone centered over the WNP. Correspondingly, the northwest flank of the anomalous anticyclonic system are controlled by the anomalous southwesterlies, which transport sufficient water vapor fluxes into the Chinese mainland, providing the favorable conditions for the occurrences of precipitation extremes, consistent with the increased trends of extreme events over China. Following the El Niño–like SST anomalies in summer, the La Niña–like SST anomalies develop in autumn, this is also accompanied by the slightly weak PDO–like SST anomalies over the Pacific. Similarly, conducive situations of the atmospheric circulations appear for the formation of extreme precipitation events.

In addition to the effects of climate variability modes, such as ENSO and PDO, the intense rainfall events over China are also modulated by local forcing factors, for example topography (Shi et al., 2008; Guo et al., 2020), and the extreme events over central-east China are also influenced by tropical cyclones (Zhang et al., 2018; Cao et al., 2019). Moreover, the strengthened greenhouse gas emissions derived from human activities during last decades also alter regional rainfall features across China (Li et al.,

2017; Ma et al., 2017). And the frequency and intensity of ENSO episodes are expected to increase under greenhouse warming (Kim et al., 2014; Cai et al., 2015). It is therefore not necessary to investigate the physical causes responsible for extreme precipitation events without considering increased greenhouse gas. In addition, the results of this study are not sensitive the selection of ENSO index, since the variations in seasonal ONI are coincident with the multivariate ENSO index 2 (Fig. S8) (Wolter and Timlin, 1998). Our works advance the understanding of the contributions of nature climate variability on the trends of precipitation extremes in China. Statistical analyses is employed in this study, the numerical simulation is a useful supplement for further explanation of variations in seasonal precipitation extremes.

Acknowledgments

We wish to thank editor, Annalisa Cherchi, for his generous encouragement for providing us with an opportunity to improve the quality of this paper. We also thank two anonymous reviewers for helpful comments that significantly improved this paper. This study is jointly supported by Natural Science Foundation and Sci-tech development project of Shandong Province (No. ZR2018MD014; J18KA210), Key research and development plan of Shandong province in 2019 (No. 2019GGX105021), Project funded by China Postdoctoral Science Foundation (No. 119100582H; 1191005830), and Project of National Natural Science Foundation of China (No. 41630532).

References

Alexander, L. V., Zhang, X., Peterson, T. C., Caesar, J., Gleason, B., Klein Tank, A., Haylock, M., Collins, D., Trewin, B., and Rahimzadeh, F. 2006. Global observed changes in daily climate extremes of temperature and precipitation, *Journal of Geophysical Research: Atmospheres*, 111. https://doi.org/10.1029/2005JD006290.

Cai, W., Van Rensch, P., Cowan, T., and Hendon, H. H. 2011. Teleconnection pathways of ENSO and the IOD and the mechanisms for impacts on Australian rainfall, *Journal of Climate*, 24, 3910-3923.

Cai, W., Wang, G., Santoso, A., McPhaden, M. J., Wu, L., Jin, F., Timmermann, A., Collins, M., Vecchi, G., and Lengaigne, M. 2015. Increased frequency of extreme La Niña events under greenhouse warming, *Nature Climate Change*, 5, 132-137.

Chen, S., Gan, T. Y., Tan, X., Shao, D., and Zhu, J. 2019. Assessment of CFSR, ERA-Interim, JRA-55, MERRA-2, NCEP-2 reanalysis data for drought analysis over China, *Climate Dynamics*, 53, 737-757.

Cao, F., Gao, T., Dan, L., Ma, Z., Chen, X., Zou, L., and Zhang, L. 2019. Synoptic-scale atmospheric circulation anomalies associated with summertime daily precipitation extremes in the middle‐lower reaches of the Yangtze River Basin, *Climate Dynamics*, 53, 3109-3129.

Cao, F., Gao, T., Dan, L., Xie, L., and Gong, X. 2019. Variability of Summer Precipitation Events Associated with Tropical Cyclones over Mid-Lower Reaches of Yangtze River Basin: Role of the El Niño‐Southern Oscillation, *Atmosphere*, 10, 256. https://doi.org/10.3390/atmos10050256.

Cao, F., and Gao, T. 2019. Effect of climate change on the centennial drought over China using high-resolution NASA-NEX downscaled climate ensemble data, *Theoretical and Applied Climatology*, 138, 1189-1202.

Chan, J. C., and Zhou, W. 2005. PDO, ENSO and the early summer monsoon rainfall over south China, *Geophysical Research Letters*, 32. doi:10.1029/2004GL022015.

Chen, G., Ming, Y., Singer, N. D., and Lu, J. 2011. Testing the Clausius‐Clapeyron constraint on the aerosol‐induced changes in mean and extreme precipitation, *Geophysical Research Letters*, 38. doi: https://doi.org/10.1029/2010GL046435.

Chen, Y., and Zhai, P. 2015. Synoptic‐scale precursors of the East Asia/Pacific teleconnection pattern responsible for persistent extreme precipitation in the Yangtze River Valley, *Quarterly*

Journal of the Royal Meteorological Society, 141, 1389-1403.

Ding, Y., Sun, Y., Wang, Z., Zhu, Y., and Song, Y. 2009. Inter‐decadal variation of the summer precipitation in China and its association with decreasing Asian summer monsoon Part II: Possible causes, *International Journal of Climatology*, 29, 1926-1944.

Donat, M. G., Lowry, A. L., Alexander, L. V., O Gorman, P. A., and Maher, N. 2016. More extreme precipitation in the world [rsquor] s dry and wet regions, *Nature Climate Change*, 6, 508-513.

Easterling, D. R., Meehl, G. A., Parmesan, C., Changnon, S. A., Karl, T. R., and Mearns, L. O. 2000. Climate extremes: observations, modeling, and impacts, *Science*, 289, 2068. doi: 10.1126/science.289.5487.2068.

Fan, J., Wang, Y., Rosenfeld, D., and Liu, X. 2016. Review of aerosol‐cloud interactions: Mechanisms, significance, and challenges, *Journal of The Atmospheric Sciences*, 73, 4221-4252.

Fu, X., Kuo, C. C., and Gan, T. Y. 2015. Change point analysis of precipitation indices of Western Canada, *International Journal of Climatology*, 35, 2592-2607.

Gao, T., Wang, H. J., and Zhou, T. 2017. Changes of extreme precipitation and nonlinear influence of climate variables over monsoon region in China, *Atmospheric Research*, 197, 379-389.

Gao, T., Xie, L., and Liu, B. 2016. Association of extreme precipitation over the Yangtze River Basin with global air‐sea heat fluxes and moisture transport, *International Journal of Climatology*, 36, 3020-3038.

Gao, T., and Wang, H. 2017. Trends in precipitation extremes over the Yellow River basin in North China: Changing properties and causes, *Hydrological Processes*, 31, 2412-2428.

Gao, T., and Xie, L. 2016. Spatiotemporal changes in precipitation extremes over Yangtze River basin, China, considering the rainfall shift in the late 1970s, *Global and Planetary Change*, 147, 106-124.

Gao, T., Luo, M., Lau, N. C., and Chan, T. O. 2020. Spatially distinct effects of two El Niño types on summer heat extremes in China, *Geophysical Research Letters*, 47, e2020G-e86982G, https://doi.org/10.1029/2020GL086982.

Gong, D., and Wang, S. 1999. Impacts of ENSO on rainfall of global land and China, *Chinese Sci Bull*, 44, 852-857.

Guan, Y., Zheng, F., Zhang, X., and Wang, B. 2017. Trends and variability of daily precipitation and extremes during 1960‐2012 in the Yangtze River Basin, China, *International Journal of*

Climatology, 37, 1282-1298.

Guo, Q., Cheng, S., Qin, W., Ning, D., Shan, Z., and Yin, Z. 2020. Vertical variation and temporal trends of extreme precipitation indices in a complex topographical watershed in the Hengduan Mountain Region, China, *International Journal of Climatology*, 40, 3250-3267.

Harada Y, Kamahori H, Kobayashi C, Endo H, Kobayashi S, Ota Y, Onoda H, Onogi K, Miyaoka K, Takahashi A, K .2016. The Jra-55 Reanalysis: Representation of Atmospheric Circulation and Climate Variability. *Journal of the Meteorological Society of Japan. Ser. II*, 94:269–302

Hoerling, M. P., Kumar, A., and Xu, T. 2001. Robustness of the nonlinear climate response to ENSO's extreme phases, *Journal of Climate*, 14, 1277-1293.

Huang, R., Liu, Y., and Feng, T. 2013. Interdecadal change of summer precipitation over Eastern China around the late-1990s and associated circulation anomalies, internal dynamical causes, *Chinese Science Bulletin*, 58, 1339-1349.

Jiang, F., Hu, R., Wang, S., Zhang, Y., and Tong, L. 2013. Trends of precipitation extremes during 1960–2008 in Xinjiang, the Northwest China, *Theoretical and Applied Climatology*, 111, 133-148.

Kim, S. T., Cai, W., Jin, F., Santoso, A., Wu, L., Guilyardi, E., and An, S. 2014. Response of El Niño sea surface temperature variability to greenhouse warming, *Nature Climate Change*, 4, 786-790.

Lau, K. M., Lee, J. Y., Kim, K. M., and Kang, I. S. 2004. The North Pacific as a regulator of summertime climate over Eurasia and North America, *Journal of Climate*, 17, 819-833.

Lehmann, J., Coumou, D., and Frieler, K. 2015. Increased record-breaking precipitation events under global warming, *Climatic Change*, 132, 501-515.

Li, H., Chen, H., and Wang, H. 2017. Effects of anthropogenic activity emerging as intensified extreme precipitation over China, *Journal of Geophysical Research: Atmospheres*, 122, 6899-6914.

Li, T. I., Bin, W., Bo, W. U., Tianjun, Z., and Chih-Pei Chang, R. Z. 2017. Theories on Formation of an Anomalous Anticyclone in Western North Pacific during El Niño: A Review, *Journal of Meteorological Research*, 31, 987-1006.

Li, J., Dong, W., and Yan, Z. 2012. Changes of climate extremes of temperature and precipitation in summer in eastern China associated with changes in atmospheric circulation in East Asia

during 1960–2008, *Chinese Science Bulletin*, 57, 1856-1861.

Lin, L., Wang, Z., Xu, Y., and Fu, Q. 2016. Sensitivity of precipitation extremes to radiative forcing of greenhouse gases and aerosols, *Geophysical Research Letters*, 43, 9860-9868.

Liu, R., Liu, S. C., Cicerone, R. J., Shiu, C., Li, J., Wang, J., and Zhang, Y. ,2015. Trends of extreme precipitation in eastern China and their possible causes, *Advances in Atmospheric Sciences*, 32, 1027-1037.

Ma, S., Zhou, T., Stone, D. A., Polson, D., Dai, A., Stott, P. A., von Storch, H., Qian, Y., Burke, C., and Wu, P. 2017. Detectable anthropogenic shift toward heavy precipitation over eastern China, *Journal of Climate*, 30, 1381-1396.

Mantua, N. J., Hare, S. R., Zhang, Y., Wallace, J. M., and Francis, R. C. 1997. A Pacific interdecadal climate oscillation with impacts on salmon production, *Bulletin of the American Meteorological Society*, 78, 1069-1080.

Miao, C., Duan, Q., Sun, Q., Lei, X., and Li, H. 2018. Non-uniform changes in different categories of precipitation intensity across China and the associated large-scale circulations, *Environmental Research Letters*, 14. https://doi.org/10.1088/1748-9326/aaf306.

Min, S., Zhang, X., Zwiers, F. W., and Hegerl, G. C. 2011. Human contribution to more-intense precipitation extremes, *Nature*, 470, 378-381.

New, M., Lister, D., Hulme, M., and Makin, I. 2002. A high-resolution data set of surface climate over global land areas, *Climate Research*, 21, 1-25.

Ouyang, R., Liu, W., Fu, G., Liu, C., Hu, L., and Wang, H. 2014. Linkages between ENSO/PDO signals and precipitation, streamflow in China during the last 100 years, *Hydrology and Earth System Sciences*, 18, 3651-3661.

Peng, D., and Zhou, T. 2017. Why was the arid and semiarid northwest China getting wetter in the recent decades? *Journal of Geophysical Research: Atmospheres*, 122, 9060-9075.

Rosenfeld, D., Sherwood, S., Wood, R., and Donner, L. 2014. Climate effects of aerosol-cloud interactions, *Science*, 343, 379-380.

Rayner, N. A., Parker, D. E., Horton, E. B., Folland, C. K., Alexander, L. V., Rowell, D. P., Kent, E. C., and Kaplan, A. 2003. Global analyses of sea surface temperature, sea ice, and night marine air temperature since the late nineteenth century, *Journal of Geophysical Research: Atmospheres*, 108.4407, https://doi.org/10.1029/2002JD002670.

Shi, X., Wang, Y., and Xu, X. 2008. Effect of mesoscale topography over the Tibetan Plateau on summer precipitation in China: A regional model study, *Geophysical Research Letters*, 35. https://doi.org/10.1029/2008GL034740.

Si, D., and Ding, Y. 2016. Oceanic forcings of the interdecadal variability in East Asian summer rainfall, *Journal of Climate*, 29, 7633-7649.

Sun, B., and Wang, H. 2015. Inter-decadal transition of the leading mode of inter-annual variability of summer rainfall in East China and its associated atmospheric water vapor transport, *Climate Dynamics*, 44, 2703-2722.

Sun, J., and Zhang, F. 2017. Daily extreme precipitation and trends over China, *Science China Earth Sciences*, 60, 2190-2203.

Sun, J. S. 2012. The contribution of extreme precipitation to the total precipitation in China, *Atmospheric and Oceanic Science Letters*, 5, 499-503.

Utsumi, N., Seto, S., Kanae, S., Maeda, E. E., and Oki, T. 2011. Does higher surface temperature intensify extreme precipitation? *Geophysical Research Letters*, 38. https://doi.org/10.1029/2011GL048426.

Wang, B., Wu, R., and Fu, X. 2000. Pacific-East Asian teleconnection: how does ENSO affect East Asian climate? *Journal of Climate*, 13, 1517-1536.

Wang, B., Zhang, M., Wei, J., Wang, S., Li, X., Li, S., Zhao, A., Li, X., and Fan, J. 2013. Changes in extreme precipitation over Northeast China, 1960 – 2011, *Quaternary International*, 298, 177-186.

Wang, B., and Zhang, Q. 2002. Pacific – east Asian teleconnection. Part II: How the Philippine Sea anomalous anticyclone is established during El Nino development, *Journal of Climate*, 15, 3252-3265.

Wang, H., Gao, T., and Xie, L. 2019. Extreme precipitation events during 1960 – 2011 for the Northwest China: space-time changes and possible causes, *Theoretical and Applied Climatology*, 137, 977-995.

Wang, H., Shao, Z., Gao, T., Zou, T., Liu, J., and Yuan, H. 2016. Extreme precipitation event over the Yellow Sea western coast: Is there a trend? *Quaternary International*, 441. https://doi.org/10.1016/j.quaint.2016.08.014.

Wang, T., Wang, H. J., Otterå, O. H., Gao, Y. Q., Suo, L. L., Furevik, T., and Yu, L. 2013

Anthropogenic agent implicated as a prime driver of shift in precipitation in eastern China in the late 1970s, *Atmospheric Chemistry and Physics*, 13, 12433. doi:10.5194/acp-13-12433-2013.

Westra, S., Alexander, L. V., and Zwiers, F. W. 2013. Global increasing trends in annual maximum daily precipitation, *Journal of Climate*, 26, 3904-3918.

Wang, Y., and Yan, Z. 2011. Changes of frequency of summer precipitation extremes over the Yangtze River in association with large-scale oceanic-atmospheric conditions, *Advances in Atmospheric Sciences*, 28, 1118. https://doi.org/10.1007/s00376-010-0128-7.

Wu J, Gao X. J. 2013. A gridded daily observation dataset over China region and comparison with other datasets. *Chinese Journal of Geophysics*, 56:1102–1111. https://doi.org/10.6038/cig20130406.

Wolter, K., and Timlin, M. S. 1998. Measuring the strength of ENSO events: How does 1997/98 rank? *Weather*, 53, 315-324.

Xiao, M., Zhang, Q., and Singh, V. P. 2015. Influences of ENSO, NAO, IOD and PDO on seasonal precipitation regimes in the Yangtze River basin, China, *International Journal of Climatology*, 35, 3556-3567.

Xiao, M., Zhang, Q., and Singh, V. P. 2017. Spatiotemporal variations of extreme precipitation regimes during 1961–2010 and possible teleconnections with climate indices across China, *International Journal of Climatology*, 37, 468-479.

Xu, Z., Fan, K., and Wang, H. 2015. Decadal variation of summer precipitation over China and associated atmospheric circulation after the late 1990s, *Journal of Climate*, 28, 4086-4106.

Yan, Y., Wu, H., Gu, G., Ward, P. J., Luo, L., Li, X., Huang, Z., and Tao, J. 2020. Exploring the ENSO Impact on Basin‐Scale Floods Using Hydrological Simulations and TRMM Precipitation, *Geophysical Research Letters*, 47, e2020G-e89476G, https://doi.org/10.1029/2020GL089476.

You, Q., Kang, S., Aguilar, E., Pepin, N., Flügel, W., Yan, Y., Xu, Y., Zhang, Y., and Huang, J. 2011. Changes in daily climate extremes in China and their connection to the large scale atmospheric circulation during 1961–2003, *Climate Dynamics*, 36, 2399-2417.

Yu, L., Zhong, S., Heilman, W. E., and Bian, X. 2018. Trends in seasonal warm anomalies across the contiguous United States: contributions from natural climate variability, *Scientific reports*, 8, 1-13.

Yu, L., Zhong, S., Pei, L., Bian, X., and Heilman, W. E. 2016. Contribution of large-scale circulation

anomalies to changes in extreme precipitation frequency in the United States, *Environmental Research Letters*, 11, 44003. doi:10.1088/1748-9326/11/4/044003.

Zhai, P., Zhang, X., Wan, H., and Pan, X. 2005. Trends in total precipitation and frequency of daily precipitation extremes over China, *Journal of Climate*, 18, 1096-1108.

Zhang, Q., Lai, Y., Gu, X., Shi, P., and Singh, V. P. 2018. Tropical Cyclonic Rainfall in China: Changing Properties, Seasonality, and Causes, *Journal of Geophysical Research: Atmospheres*, 123, 4476-4489.

Zhang, X., Wan, H., Zwiers, F. W., Hegerl, G. C., and Min, S. K. 2013. Attributing intensification of precipitation extremes to human influence, *Geophysical Research Letters*, 40, 5252-5257.

Zhu, Y., Wang, H., Ma, J., Wang, T., and Sun, J. 2015. Contribution of the phase transition of Pacific Decadal Oscillation to the late 1990s' shift in East China summer rainfall, *Journal of Geophysical Research: Atmospheres*, 120, 8817-8827.

Figure captions

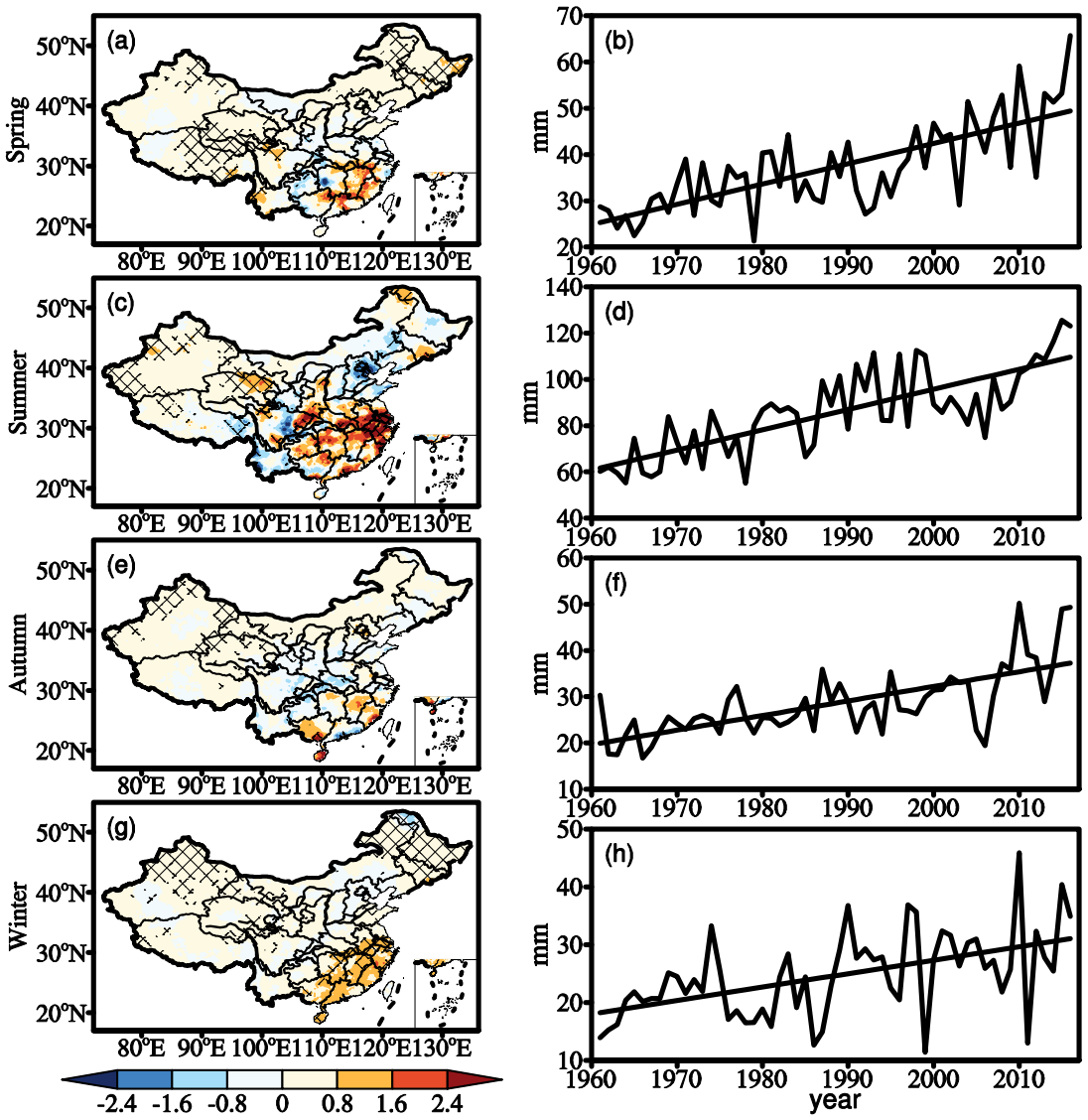

Figure 1. The spatial patterns of trends (left panel) and time series (right panel) of the amount of daily cumulative rainfall amount exceeds the 90th percentile (R90p) during 1961-2016. Hatching denotes the areas with statistical significance at the 95% confidence level (Unit: mm/yr). Time series are averaged over all gridded sites with increasing trends being statistically significant at the 95% confidence level. Each row represents a season as labelled in the left.

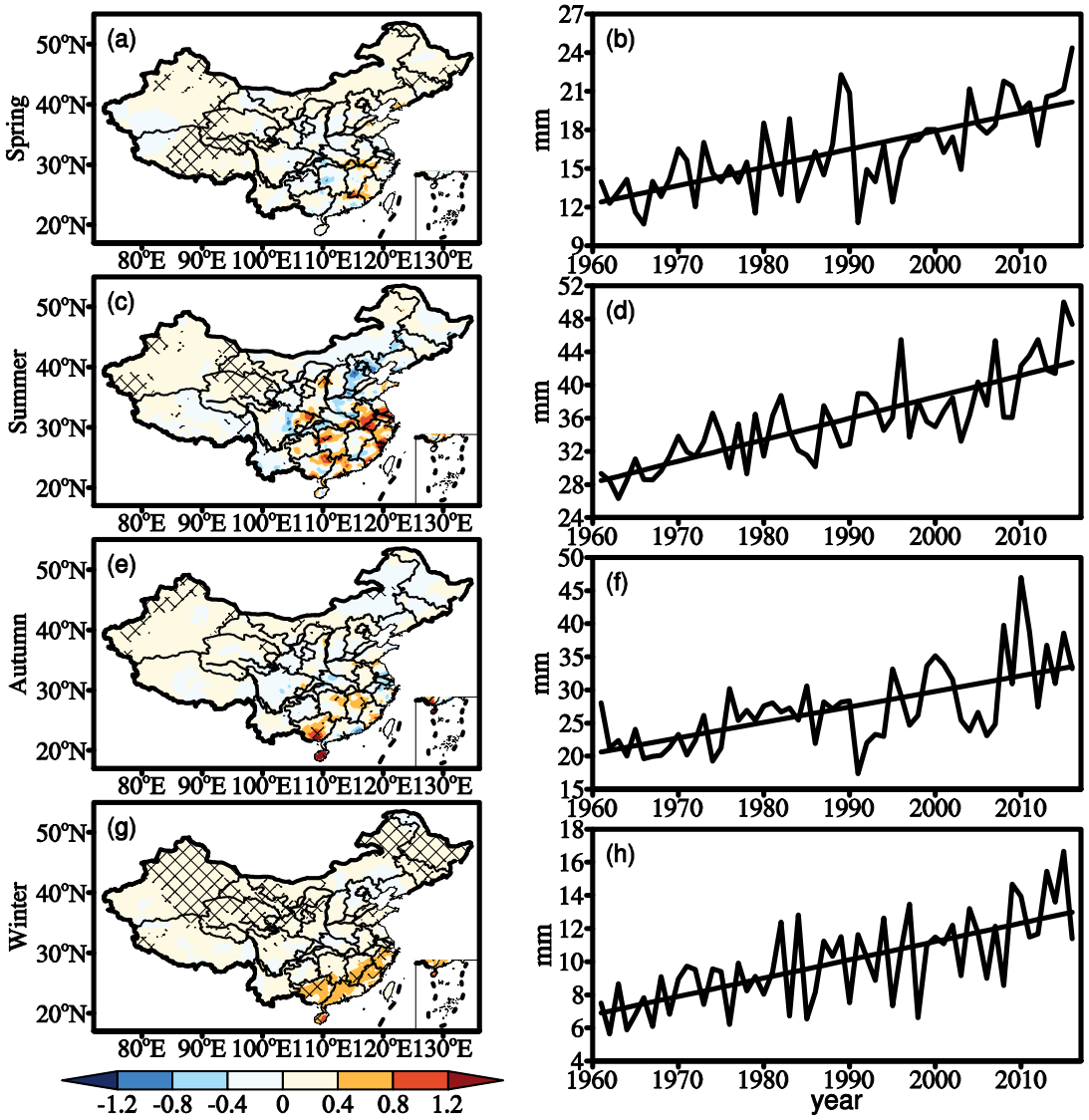

Figure 2. The same as Figure 1, but for maximum consecutive 5-day precipitation (RX5day).

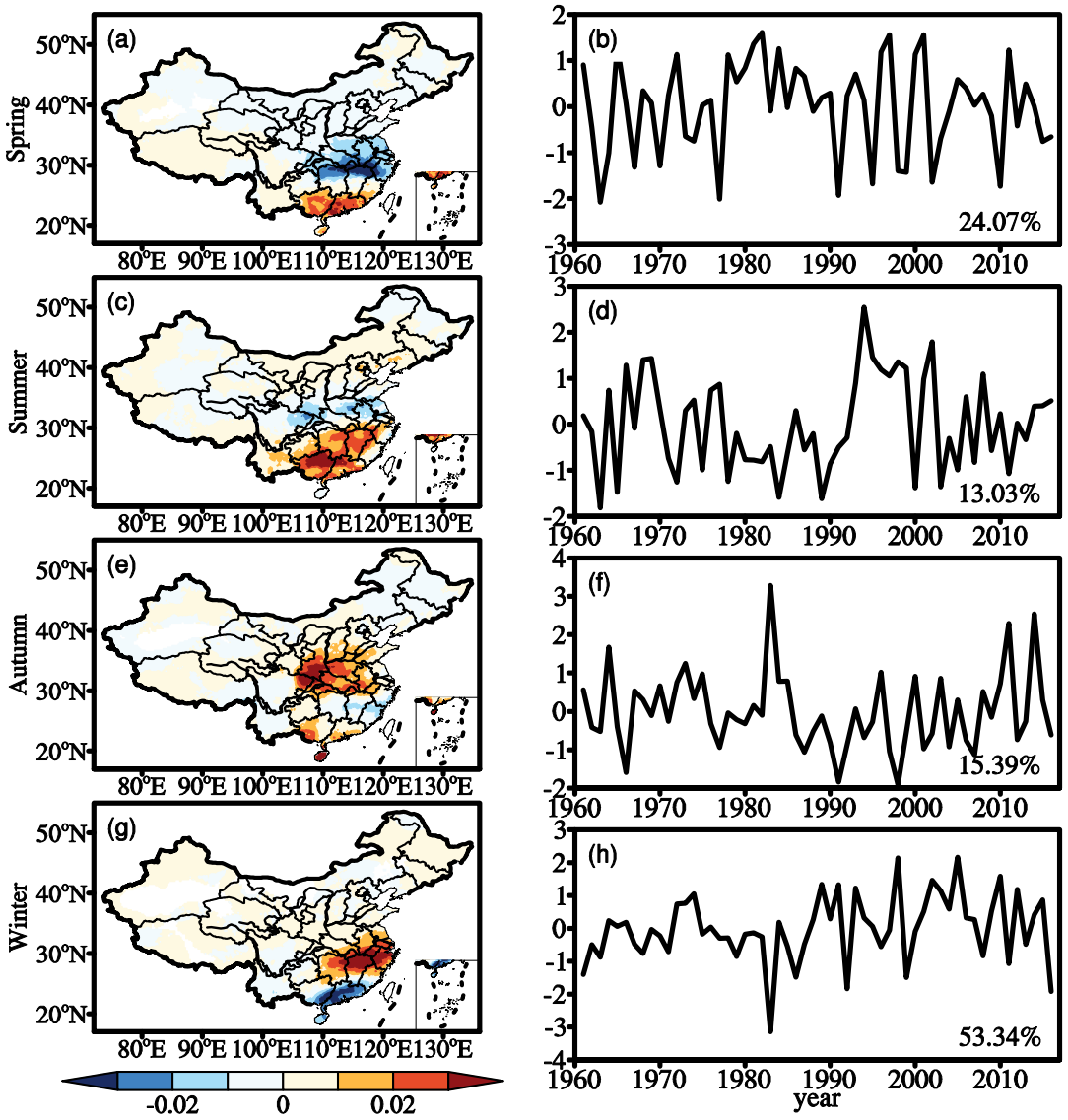

Figure 3. The spatial patterns of empirical orthogonal function (EOF, left panel) and principal components (PCs, right panel) for the R90p. The percentages in right panel represent total variances of the first modes at the seasonal scale.

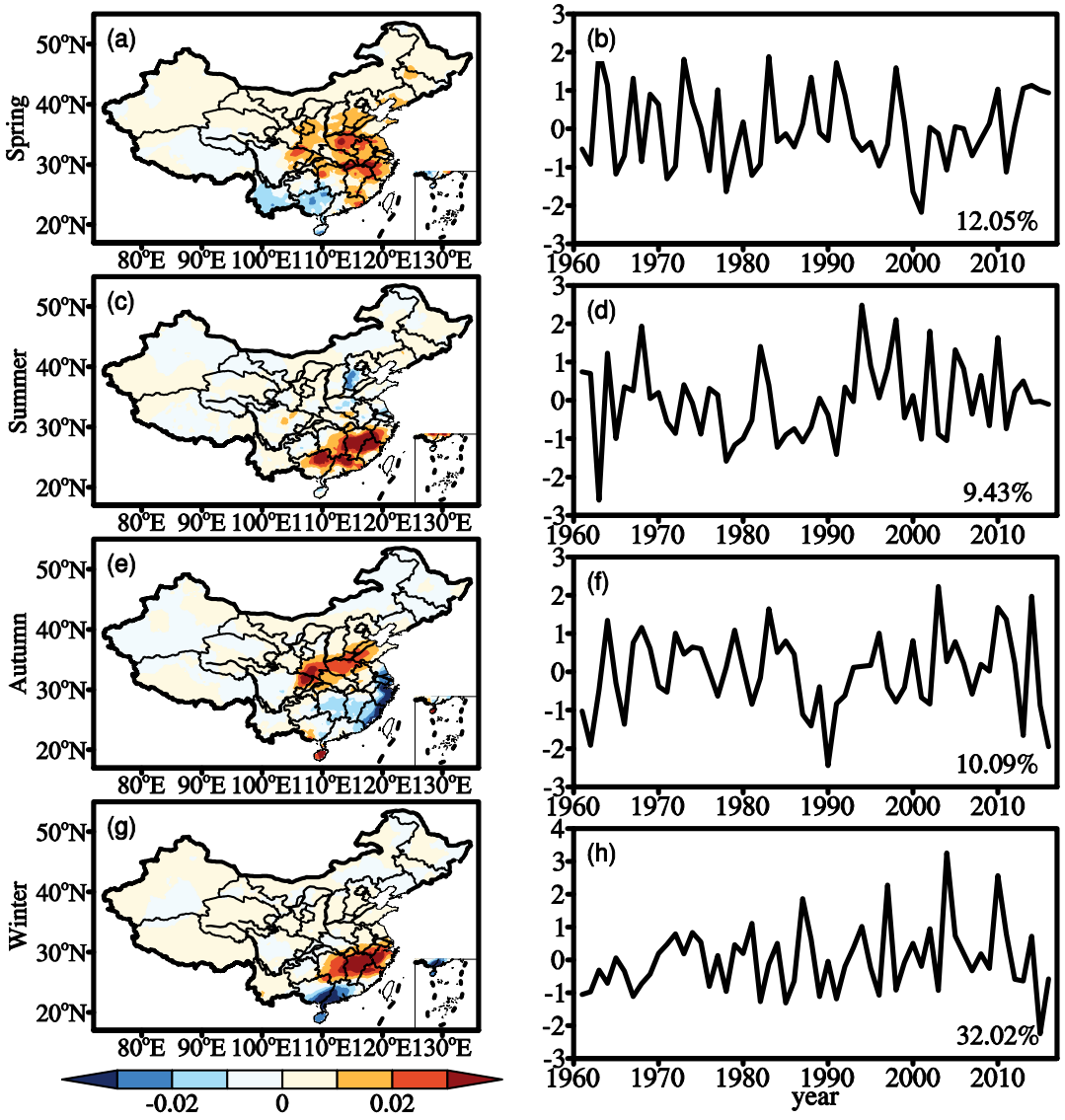

Figure 4. The same as Figure 3, but for RX5day.

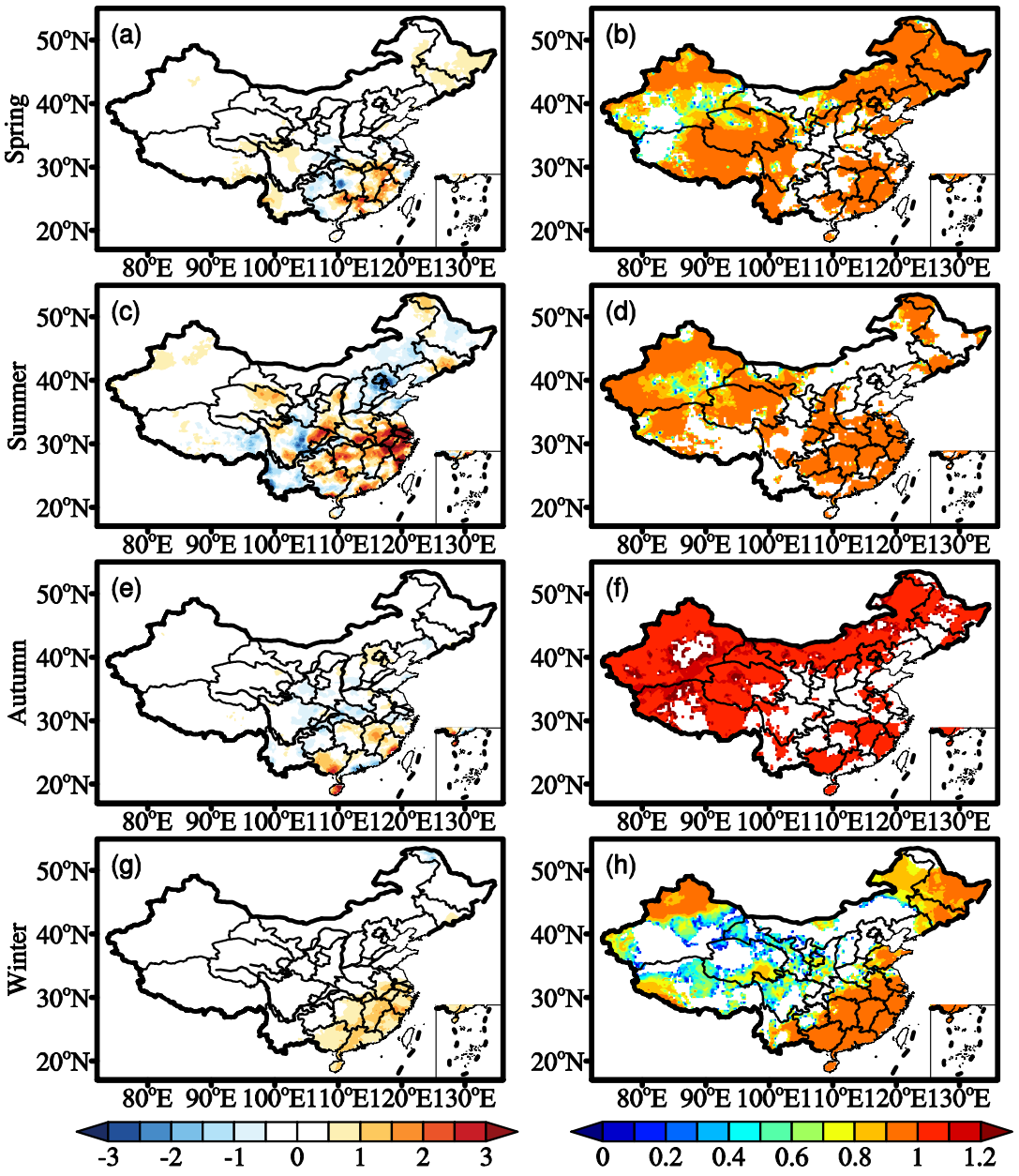

Figure 5. The spatial patterns of residual trends (left panel) and ratios of residual trends to total trends (right panel) of the R90p. Unit: mm/yr.

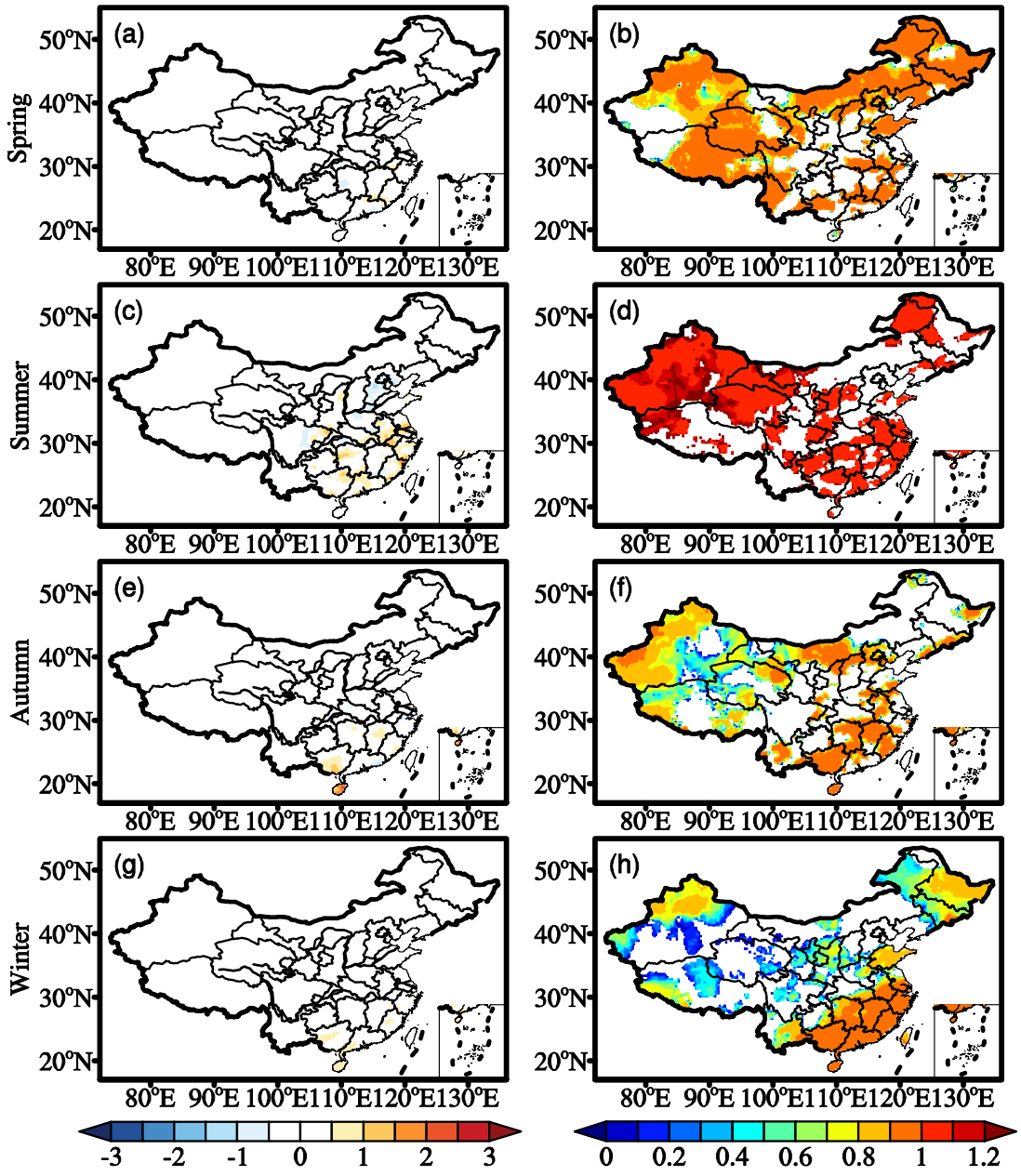

Figure 6. The same as Figure 5, but for RX5day.

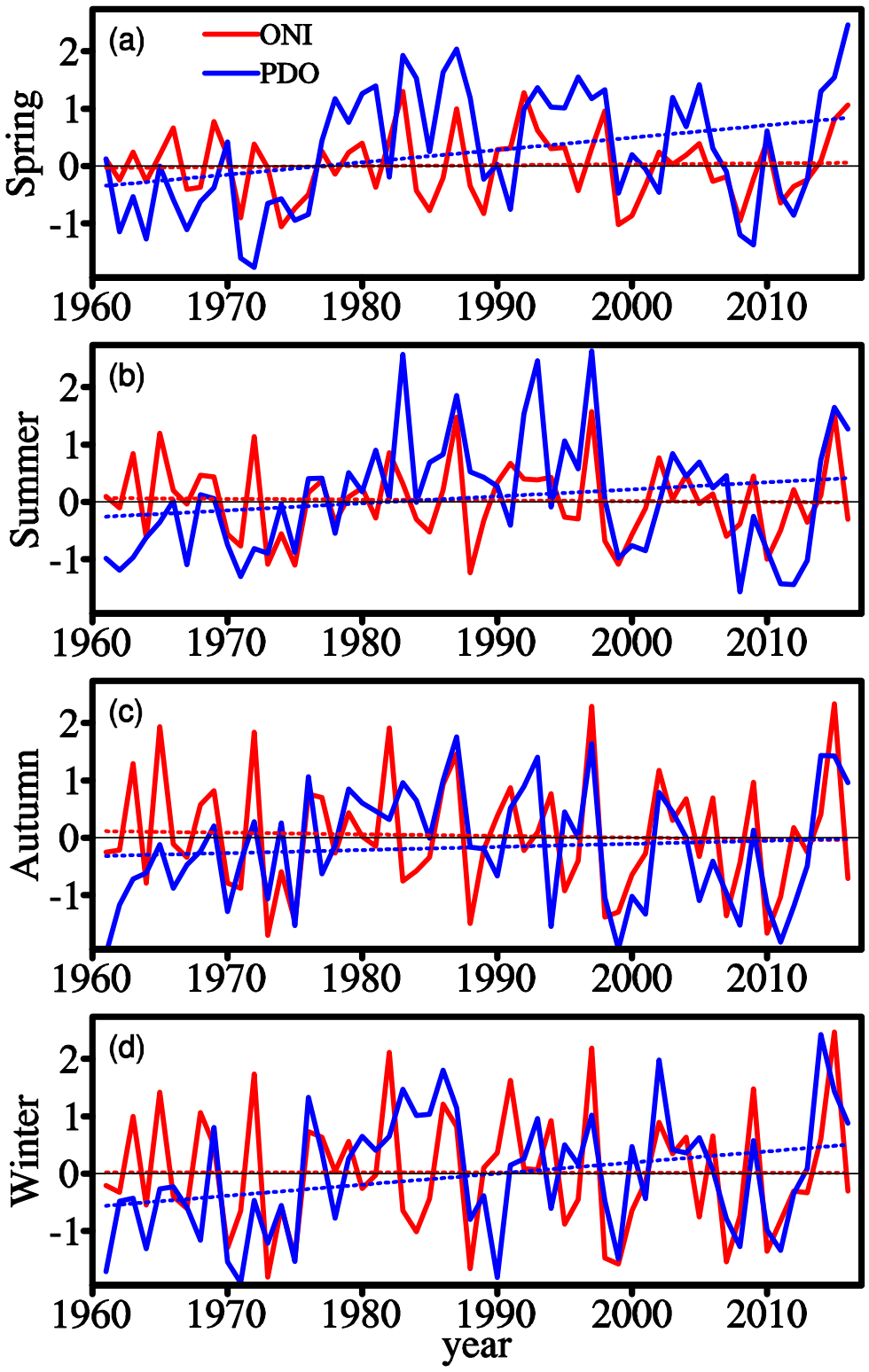

Figure 7. The time series of the normalized ENSO (represented by ONI) and PDO indices. Dashed lines denote their trends, and the black lines denote zero.

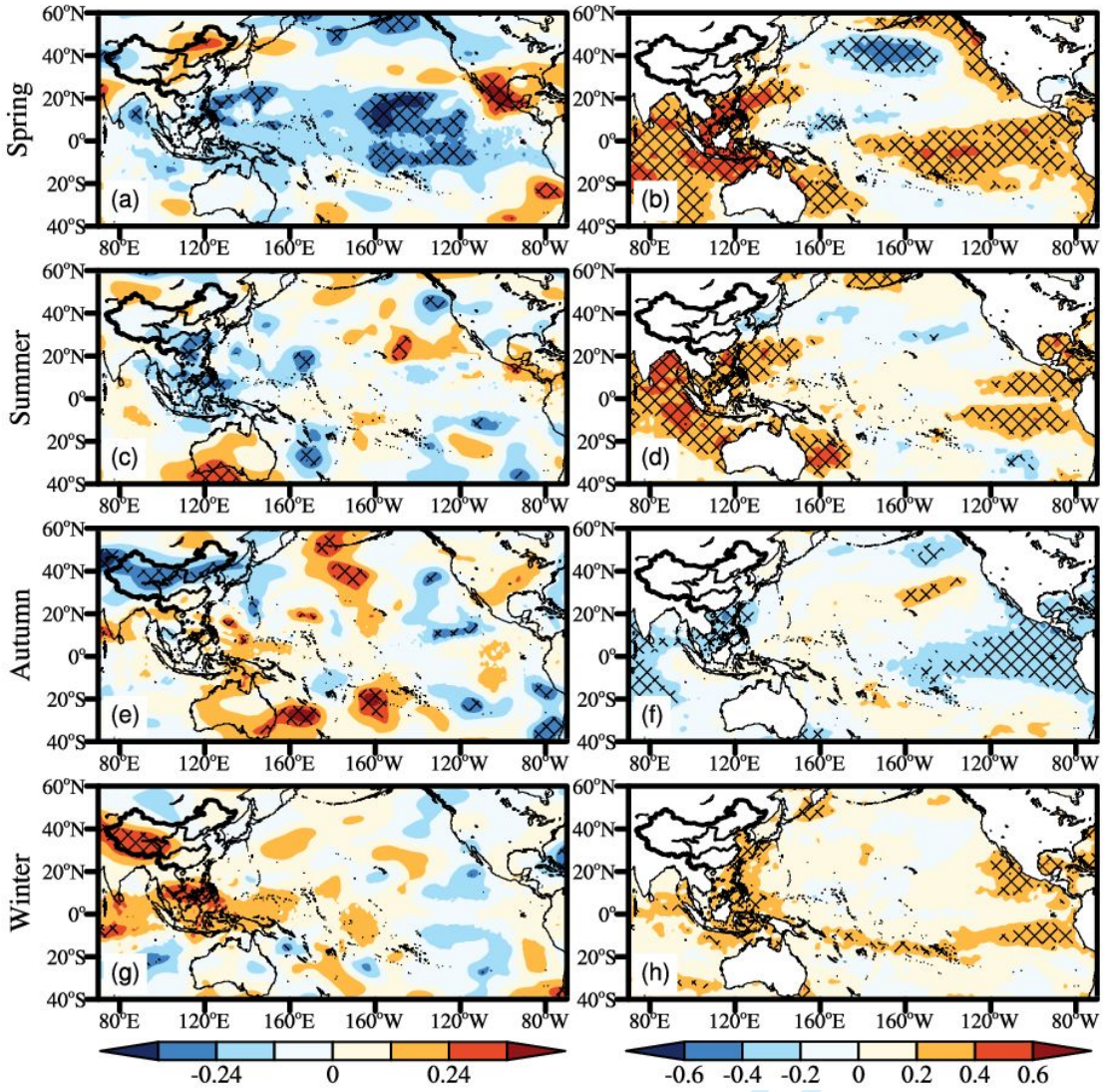

Figure 8. The anomalous geopotential height at 500 hPa (left column) and sea surface temperature (right column) regressed to the PC1s of the number of the R90p during 1961-2016. Hatching denotes the areas with statistical significance at the 95% confidence level.

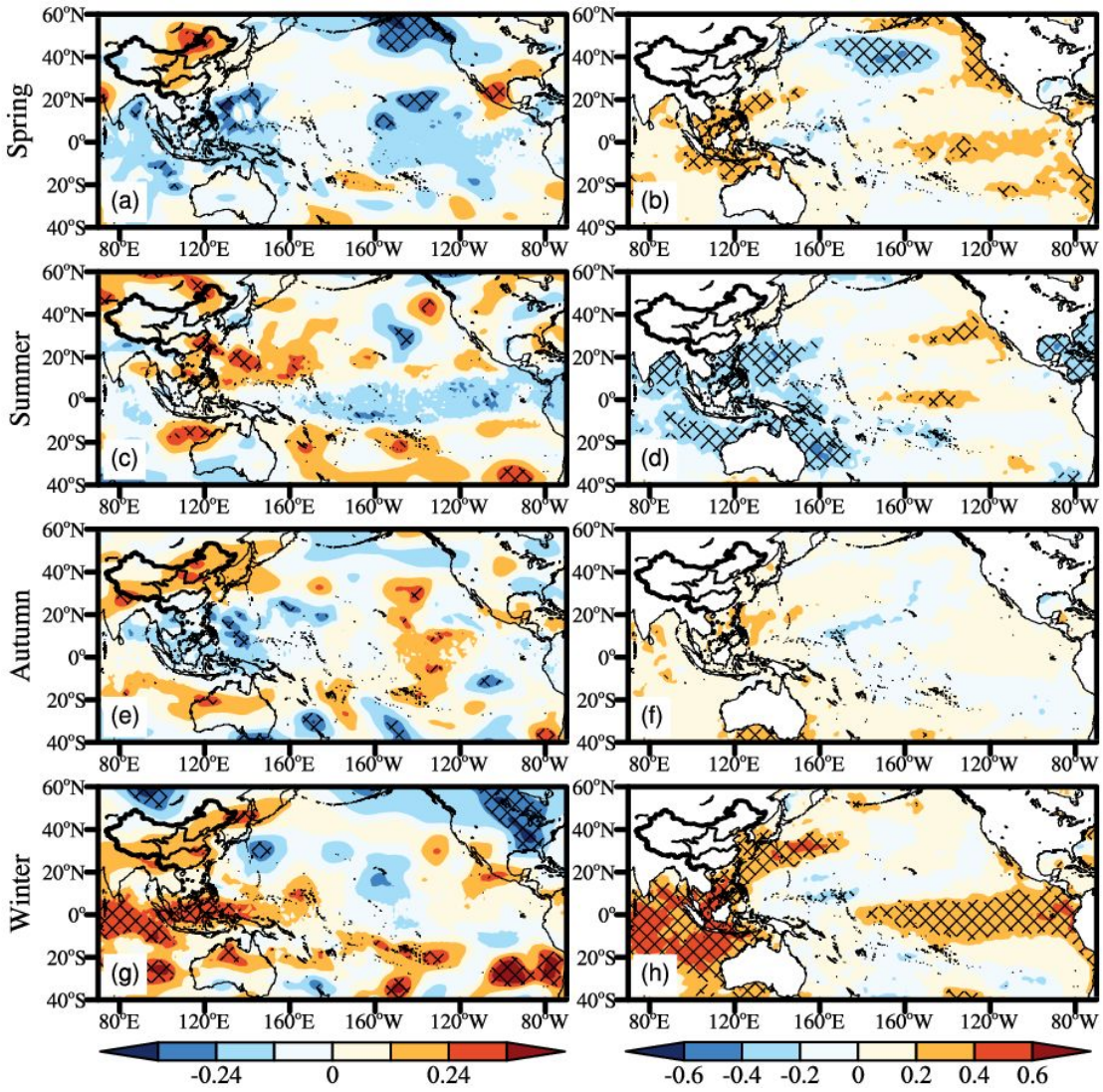

Figure 9. The same as Figure 8, but for RX5day.

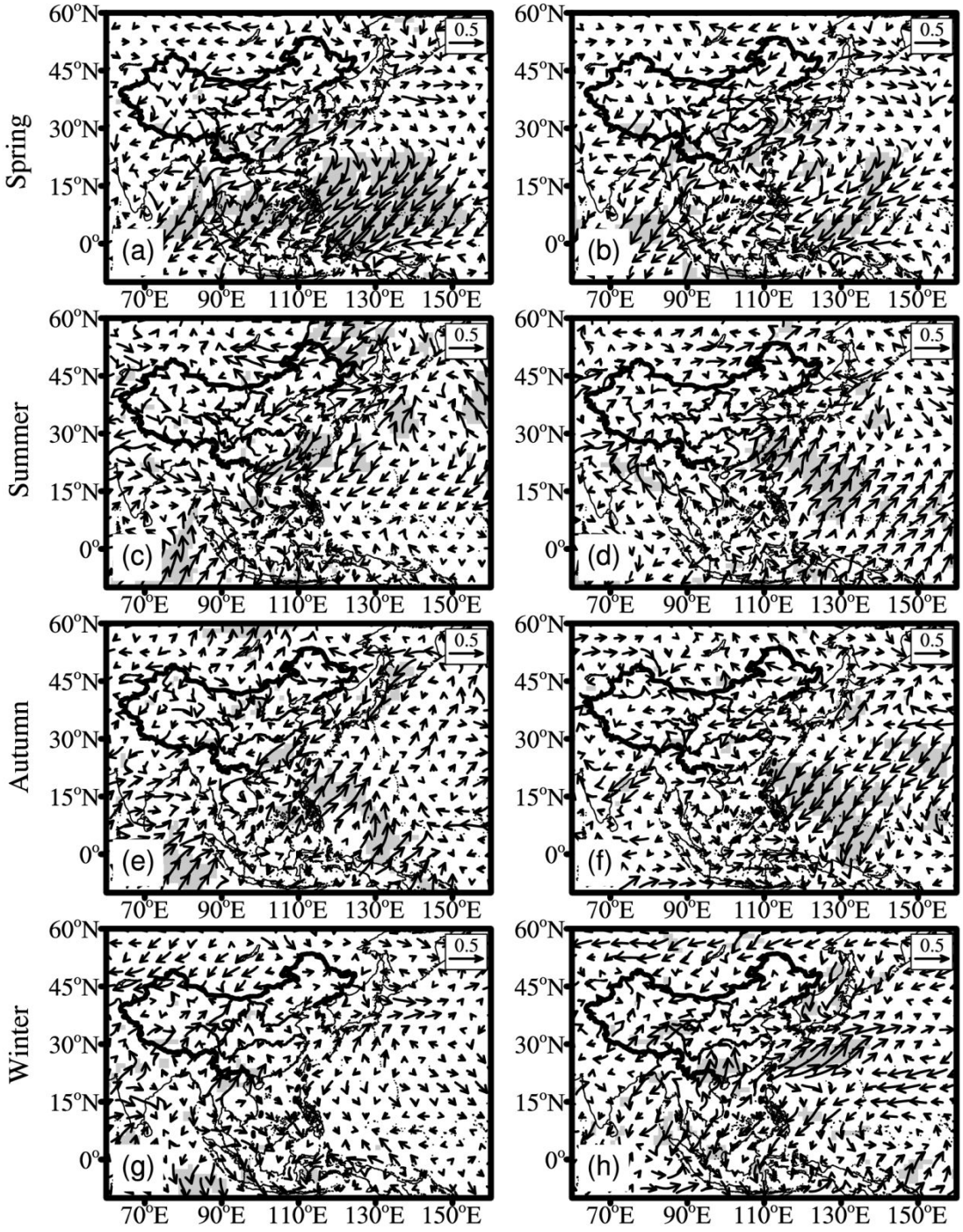

Figure 10. The wind field at 850 hPa regressed to the PC1s of the R90p (left column) and RX5day (right column) during 1961-2016. Shading denotes the areas with statistical significance at the 90% confidence level.

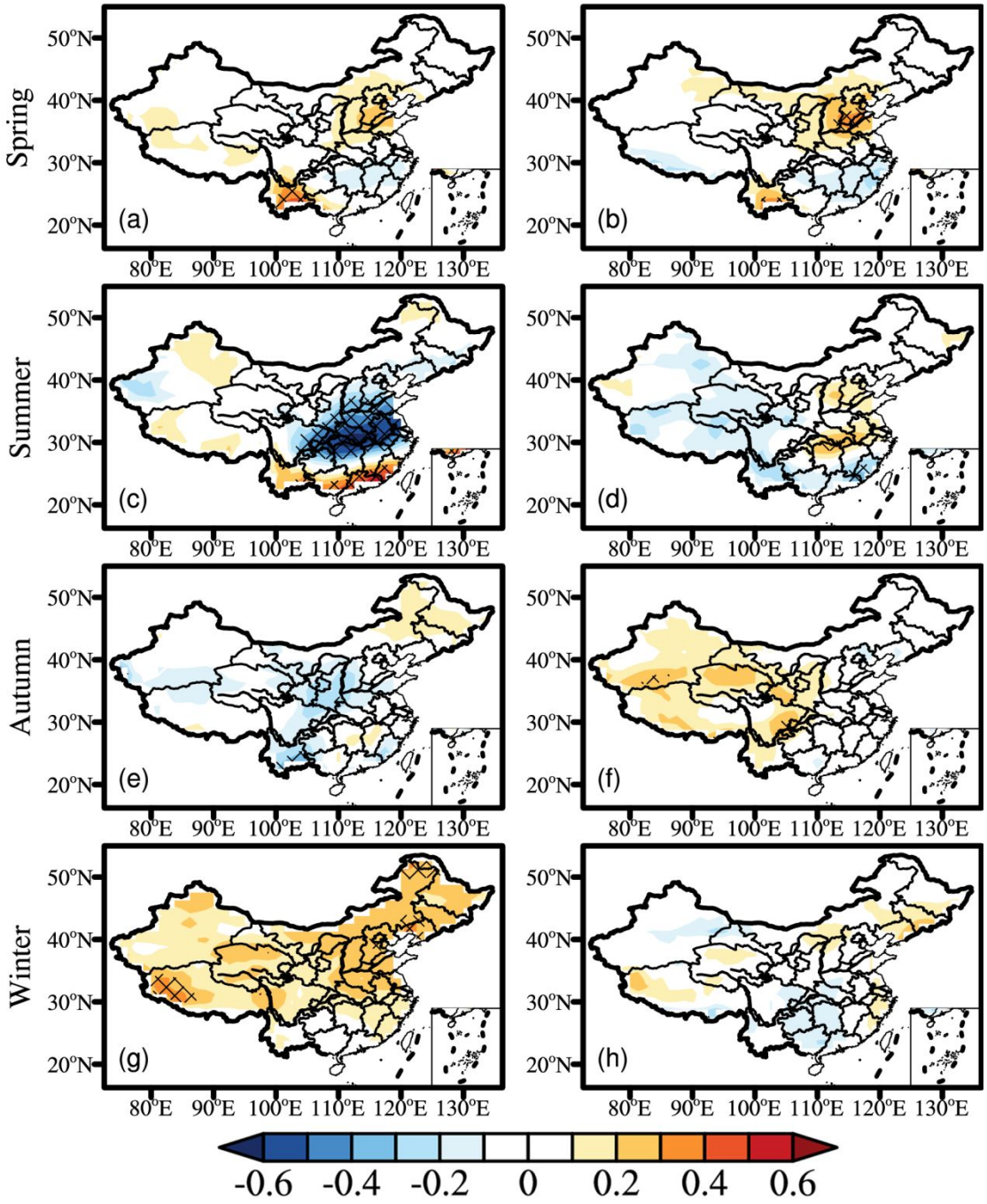

Figure 11. The same as Figure 10, but for 2-m temperature.

Table caption

Table 1. Coefficients of multivariate regression between seasonal PC1s for precipitation extremes and the ENSO as well as PDO indices.

Index	R90p				RX5day			
	Spring	Summer	Autumn	Winter	Spring	Summer	Autumn	Winter
ONI	0.0903	-0.1327	-0.2702	-0.0479	0.0612	0.4428	0.0367*	0.3239
PDO	0.3569*	0.2642	0.0381*	0.1160	0.3051*	-0.1129	-0.0739	-0.0449

*denotes the coefficients are statistically significant at the 90% confidence level.